J. Appl. Comput. Mech., 9(1) (2023) 181-194
DOI: 10.22055/jacm.2022.40704.3644

ISSN: 2383-4536
jacm.scu.ac.ir

Shahid Chamran University of Ahvaz

Journal of Applied and Computational Mechanics

Research Paper

A Reduced-Order Simulation Methodology for Nanosecond-Pulsed Plasmas in a Backward-Facing Step Supersonic Combustor Configuration

Luis F. Alvarez[1], Albio D. Gutierrez[2]

[1] Aerospace Exploration and Development Research Group - IDEXA, Universidad del Valle, Cl 13 # 100-00, E33-1009, 760032, Cali, Colombia, Email: luis.fernando.alvarez@correounivalle.edu.co

[2] Research Group in Fatigue and Surfaces, Universidad del Valle, Cl 13 # 100-00, E49-2011, 760032, Cali, Colombia, Email: albio.gutierrez@correounivalle.edu.co

Received May 09 2022; Revised July 15 2022; Accepted for publication July 22 2022.
Corresponding author: A.D. Gutierrez (albio.gutierrez@correounivalle.edu.co)

Abstract. This work presents a simplified methodology for coupling the physics of a nanosecond-pulsed discharge to the process of supersonic combustion within a backward-facing step combustor. The phenomena of plasma and supersonic combustion are simulated separately and then coupled. Based on results reported in the literature, a zero-dimensional plasma model is built, considering only the kinetic effects of the nanosecond-pulsed discharge. A set of Favre-averaged compressible Navier-Stokes equations, as well as finite rate chemistry, is used in the combustion model and solved with a control-volume based technique. The plasma-supersonic combustion coupling process only considers the discharge as a source of O and H radical species. The calculated densities of the radicals generated during each pulse from the plasma model are periodically seeded inside the domain of the combustor. The proposed methodology is used to perform a novel simulation that involved the application of plasma to a well-known supersonic combustion experiment. The temperature and species concentration contours show that the proposed methodology captures the main effects of the nanosecond-pulsed discharge on supersonic combustion. The ignition delay time is reduced when the plasma discharge was applied. In addition, the simulations show that the plasma causes a supersonic low-enthalpy mixture to ignite, confirming the capability of the methodology.

Keywords: Plasma assisted combustion, Nanosecond pulsed discharge, Scramjet, Supersonic flow, CFD.

1. Introduction

Supersonic and hypersonic aircraft are of particular interest due to their ability to enable low-Earth orbit flights as well as their defense and transport applications within the atmosphere [1-7]. A possible candidate for these high-speed flights is the scramjet engine. This type of engine needs to burn significant amounts of fuel to provide the thrust necessary to achieve high velocities. One of the main technical challenges that scramjets face in hypersonic flights is efficient fuel combustion [8].

When scramjets burn fuel at speeds above Mach 7, the flow residence time in the engine is shorter than the ignition delay time and the fuel consumption time of typical mixtures. As a result, the fuel-air mixture does not have enough time to autoignite and burn completely. This leads to inefficient fuel use, with the consequence that the flow may not achieve a faster speed than the incoming air. Another reason for inefficient combustion in high-speed flows is the difficulty in holding and stabilizing the flame.

To address the issue of the short flow residence time for mixing and igniting, various methods have been studied, such as adding radicals, increasing the temperature and pressure at the combustor inlet via shockwaves, changing the fuel/oxidizer mixtures and mixing enhancement [9, 10]. On the other hand, the difficulty of holding and stabilizing the flame has been addressed with various techniques, such as the utilization of bluff bodies as fuel injectors that block the flow and increase mixing through vortex generation [11-13]. Another technique is normal supersonic fuel injection, which generates bow shocks, leading to subsonic regions that promote mixing [14, 15]. In addition, cavities and steps have played key roles as flame holders, generating recirculation zones that allow the air and fuel to mix more slowly and increase the flow residence time in the combustor of the scramjet engine [16-21].

Even though all these approaches enhance combustion through shorter ignition times, increased mixing, longer residence times and increased flame holding, they are static and therefore difficult to optimize for the entire range of scramjet flight conditions, such as altitude, velocity, pressure and incoming air temperature. Furthermore, the geometric alterations used in some of these techniques can induce shockwaves in the combustor, leading to stagnation pressure losses that increase as the flight Mach number increases [22, 23].

In recent years, plasma-assisted combustion (PAC) has shown exceptional capabilities for improving ignition, flame stabilization, and fuel/air mixing via kinetical- [24-30], thermal- [31-35], and plasma-induced aerodynamic effects [36-38]. Nonequilibrium

Published online: August 03 2022

plasmas, such as corona microwave, low-pressure glow, and nanosecond high-voltage discharges, are capable of enhancing combustion by supplying active radicals in such a way that chemical reaction pathways are modified and combustion times are shortened [27]. Experimental studies have shown that the introduction of radicals reduces the ignition delay time and kinetically enhances flame stability in supersonic environments [39]. Nonetheless, in-ground flight testing of supersonic combustors is limited by cost and technical difficulties, resulting in limited test conditions. In addition, the power capability of ground facilities is insufficient for reproducing all the conditions that describe the scramjet flow field for full-scale engines (matching enthalpy and Mach numbers) [40]. As a result, computational analysis is required to gain an in-depth understanding of the phenomenon of plasma in scramjet engines and to perform rapid tests of different geometric designs and test conditions. It is worth noting that simulations and experiments complement one another. Plasma-assisted combustion in supersonic flows can be simulated using both detailed and simplified models. Detailed models involve the full coupling of plasma physics with supersonic combustion flows, which requires a high computational capacity. Simplified plasma modeling, on the other hand, focuses on the most representative plasma effects on combustion, which depend on the type of discharge simulated. For the case of nanosecond-pulsed discharges, the kinetic effects are dominant.

Detailed PAC models include fully-coupled plasma-combustion chemistry and sets of stiff equations that account for plasma species generation and transport, as well as for plasma-induced heat and forces that affect the combustion process [41]. Some of these models also include Large Eddy Simulations (LES) for turbulence modeling [42]. Despite the details of these PAC models, certain studies have provided evidence that plasma effects on combustion, such as heating, electromagnetic forces and current densities, are lower than kinetic effects in nanosecond-plasma discharges [43, 44]. In addition, detailed plasma-combustion coupled chemistry, in some cases, may be inefficient. Among the significant number of reactions involved in nonequilibrium plasma phenomena in air, it has been observed that for reduced electric field values (between 100 and 400 Td), in nanosecond-pulsed discharges, approximately 90% of the discharge power goes only into plasma reactions, leading to the dissociation of O_2 molecules [44-46] and the generation of O radicals. Furthermore, it has been shown by some studies [47, 48] that H and O radicals by the plasma are mainly responsible for reducing the ignition delay time. Bozhenkov et al. [47] studied the kinetics of plasma-combustion applying a nanosecond plasma discharge in a shock tube. The experiment separated the thermal plasma effect from the kinetic effect. It was found from this study that the plasma kinetic effect can lead to a decrease of the H_2 ignition delay time by almost one order of magnitude. This ignition delay was primarily a result of H and O produced during the discharge. Breden et al. [41, 43] performed computational studies of nanosecond pulsed discharges in supersonic flows and found that the temperature increase due to the gas heating from the discharge is rapidly dissipated as a result of the supersonic flow convection downstream.

These facts have been used by authors such as Do et al. [39] and Nagaraja [42] to develop simplified models that assume constant plasma parameters, including electric fields and gas density, while neglecting heat and magnetic contributions, as well as certain plasma reactions, for nonequilibrium discharges. Given that nanosecond-pulsed plasmas mostly yield radicals to initiate combustion reactions, Do et al. [39] neglected excited and ionized species generation and used a simplified radical yield calculation method for dissociation reactions. The model also neglected heat and plasma aerodynamic effects, which are considered to be relatively minor in comparison to kinetic effects in nonequilibrium plasmas.

Even though these simple plasma models do not predict aspects such as charged species transport or thermal or aerodynamic plasma effects, the results concerning radical generation are quite logical according to combustion enhancement experiments [39], [49-51]. Additionally, different time and length scales for nonequilibrium plasmas and supersonic flows allow for additional model simplifications [41, 43], leading to results that are relatively close to experiments.

While detailed models require expensive computations for the assembly and solution of Poisson's Equation and electron density and energy equations, with multiple processors working in parallel, simplified models eliminate these demanding calculations by making the aforementioned assumptions, requiring less computational capacity. This minimized complexity of the simplified models for nanosecond-plasma discharges is mainly due to assumptions that lead to equations that account for kinetic plasma effects while neglecting thermal and magnetic effects on combustion. Nonetheless, current simplified models, such as that of Do et al. [39, 49], also ignore important flow effects such as turbulence, fuel-oxidant mixing and compressibility. All these factors are critical in supersonic combustion and therefore influence PAC models. Although it is possible to simplify the detailed chemical and electrical properties of the plasma when modeling nonequilibrium discharges, it is also important to include turbulence and compressible flow effects in these simplified models. Consequently, the computational demand is decreased in terms of plasma. To summarize, reduced-order models that capture plasma-enhanced combustion as well as fluid flow and thermal transport at supersonic speeds could potentially reduce the computational cost involved in scramjet engine design.

Another work by Breden and Raja [41] and Do et al. [49] has provided an opportunity to develop a model that simplifies the computationally expensive terms in plasma models while also including the effects of combustion, turbulence and compressibility of supersonic reacting flows and can be tested experimentally.

Based on previous results, this work, unlike detailed plasma-assisted combustion models in the literature, proposes a unique, simplified methodology for simulating plasma in supersonic combustion by separating plasma kinetics from combustion kinetics and coupling the plasma and reacting flow phenomena solely by cyclically seeding O and H radicals into the computational flow domain. Furthermore, while some simplified plasma combustion models calculate only the plasma radical yield via short-cut estimations while ignoring mixing, turbulence and shock wave flow effects on combustion, the model proposed in this study solves plasma kinetics for a variety of species and calculates supersonic reacting flow patterns for compressible turbulence flows via CFD, resulting in more accurate results.

Additionally, the supersonic combustion experiment performed by Burrows and Kurkov [52] was simulated. This experiment has been widely simulated in various studies given the detailed data provided by the authors. Nonetheless, in this work, the proposed methodology is used to, for the first time, apply a nanosecond-pulsed discharge to this experiment and analyze the results.

2. Description of the Model

Due to the fact that the discharge and compressible reactive flow processes have different characteristic time scales, the governing equations for the nanosecond plasma discharge and the supersonic combustion phenomena are solved separately and then combined. The nanosecond-pulsed plasma discharge simulation occurs on a nanosecond scale, whereas the time-step size of the compressible reactive flow is characterized by the Courant number criteria, which is 1.2×10^{-8} s in this case. The time size step for the discharge simulation was set to 5×10^{-10} s. Therefore, one discharge pulse is shorter than a single reactive flow step. This fact also allows us to separate the plasma chemistry from the combustion chemistry.

For the plasma-flow coupling approach, it is assumed that the effect of the discharge is reduced to the seeding of O and H radicals produced by the plasma into the combustion environment, which has a significant impact on ignition. This modeling approach is based on evidence that the main effect of these radicals on combustion reactions is to drive the kinetic enhancement of the plasma during ignition [44, 47, 48]. In addition, the plasma model considers the discharge to be spatially uniform, which will be explained in Section 2.2.2. Based on this assumption, the plasma radicals are assumed to be concentrated uniformly during each electric discharge pulse only in the area of the computational combustion domain formed by the electric discharge electrodes that represent the plasma volume. Therefore, O and H radicals are uniformly seeded in this area.

The plasma modeling equations were solved using ZDPlaskin [53] and Bolsig+ [54] software, whereas the unsteady turbulent compressible reactive flow equations were solved via ANSYS Fluent software.

The proposed plasma and reacting flow modeling approaches were coupled as follows. For each flow step, the Fluent solver updated the species concentration, pressure, temperature, velocity fields and turbulence information. For each plasma pulse, the area-average flow data calculated in the discharge area were input into the plasma kinetics solver to compute the plasma species densities. Subsequently, the densities of the O and H radicals produced during the discharge were seeded into the discharge area inside the computational domain of the combustion simulation to update the flow parameters in the next flow step. Figure 1 shows the schematic of the plasma-flow coupling cycle and its relationship with the combustor domain regions. As it can be seen, the entire process is cyclic. The plasma solver needs information about the pressure, temperature and composition of the gas for Bolsig+ to calculate the reaction rate coefficients and obtain the plasma concentration. Similarly, the flow solver requires plasma-generated species information to calculate the combustion reactions and update the flow parameters.

2.1 Governing Equations

2.1.1 Governing Equations

In this work, the Favre-averaged mean mass, momentum and energy conservation equations, shown in Equations (1), (2) and (3) are used to describe the turbulent, compressible, unsteady, viscous and thermally perfect flow inside a scramjet combustor. The correlations of the fluctuating terms in these equations are modeled using the k-ε renormalization group (RNG) [55] and shear stress transport (SST) k-ω [56] models.

$$\frac{\partial\bar{\rho}}{\partial t}+\frac{\partial(\bar{\rho}\widetilde{u_p})}{\partial x_p}=0 \tag{1}$$

$$\frac{\partial(\bar{\rho}\widetilde{u_p})}{\partial t}+\frac{\partial(\bar{\rho}\widetilde{u_p}\widetilde{u_q})}{\partial x_q}=-\frac{\partial\bar{P}}{\partial x_p}+\frac{\partial}{\partial x_q}\left(\bar{\tau}_{qp}-\overline{\rho u_q{}''u_p{}''}\right) \tag{2}$$

$$\frac{\partial(\bar{\rho}\mathrm{E})}{\partial t}+\frac{\partial(\bar{\rho}\widetilde{u_q}H)}{\partial x_q}=\frac{\partial}{\partial x_q}[\mathrm{K}\frac{\partial\tilde{T}}{\partial x_q}-\sum_n\tilde{h}_nJ_{n,q}-\overline{\rho u_q''h''}+\overline{\bar{\tau}_{qp}u_i''}-\frac{\overline{\rho u_q''u_p''u_p''}}{2}+\widetilde{u_p}(\bar{\tau}_{qp}-\overline{\rho u_q{}''u_p{}''})] \quad + \quad S_h \tag{3}$$

$$E=\tilde{e}+\frac{\widetilde{u_p}\widetilde{u_p}}{2}+k \tag{4}$$

$$H=\tilde{h}+\frac{\widetilde{u_p}\widetilde{u_p}}{2}+k \tag{5}$$

$$\bar{\rho}=\frac{P_{op}+\bar{P}}{\frac{R}{M_W}\tilde{T}} \tag{6}$$

The ideal gas law was utilized to model the density of the mixture, as shown in Equation (6). The mixing and transport processes of the chemical species resulting from combustion were modeled by solving conservation equations for the local mass fractions of each species, as shown in Equation (7). Equation (9) couples Equations (3) and (7) to model the enthalpy contribution of each species to energy conservation. Equation (10) shows that this enthalpy contribution depends on both the temperature and the specific heat of each species.

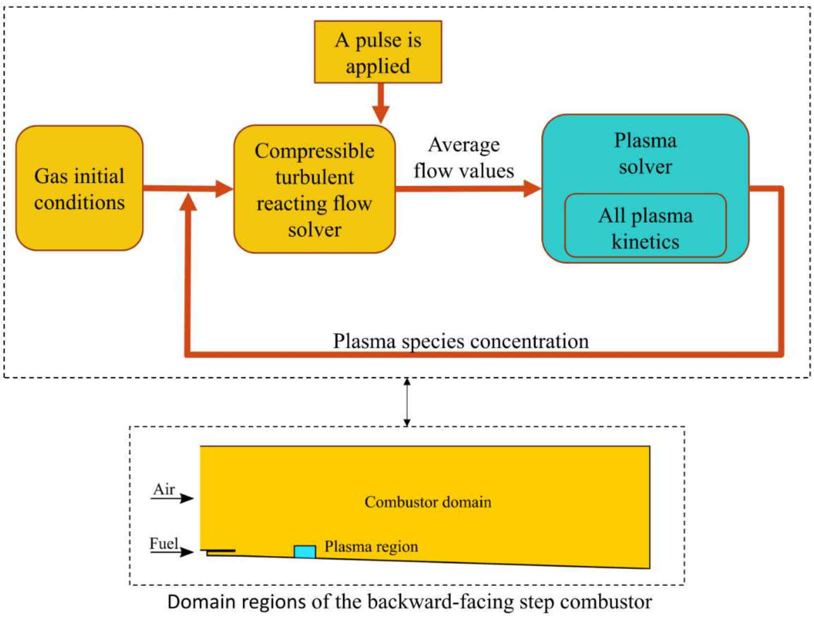

Fig. 1. Schematic of the plasma-flow coupling cycle and its relationship with the combustor domain regions.

$$\frac{\partial(\rho Y_n)}{\partial t}+\frac{\partial(\rho u_p Y_n)}{\partial x_p}=\frac{-J_{n,p}}{\partial x_p}+R_n \tag{7}$$

$$J_{n,p}=-\left(\rho D_n+\frac{\mu_t}{Sc_t}\right)\frac{\partial Y_n}{\partial x_p}-D_{T,n}\frac{1}{T}\frac{\partial \mathrm{T}}{\partial x_p} \tag{8}$$

$$h=\sum_j Y_n h_n \tag{9}$$

$$h_n=\int_{Tref}^{T} c_{p,n}dT \tag{10}$$

To account for the production of chemical species from combustion reactions, the second term on the right-hand side of Equation (7) was defined according to the laminar finite rate model described in Equation (11).

The reaction rates were determined via the Arrhenius law, as shown in Equation (15). Both third-body efficiencies and Arrhenius parameters were defined by the authors of the selected reaction mechanisms [57, 58]. This approach allowed for the calculation of multiple-step kinetic mechanisms, which permitted to capture the effect of active radicals on the chain-branching process. Radicals such as O, H and OH must react with other species to appropriately model combustion and plasma. Thus, multistep chemistry needs to be modeled over turbulent–chemistry interactions. While the reacting flow model presented in this work ignores the effect of turbulence on the production of species, supersonic flames are characterized by slower chemistry and smaller turbulence-chemistry interactions than subsonic flames [59].

$$R_n=M_{W,n}\sum_{r=1}^{N_R}\widehat{R_{n,r}} \tag{11}$$

$$\sum_{i=1}^{N}v'_{n,r}\mathcal{M}_n \overset{kf_r}{\rightarrow} \sum_{n=1}^{N}v''_{n,r}\mathcal{M}_n \tag{12}$$

$$\widehat{R_{n,r}}=\Gamma_{tb}\left(v''_{n,r}-v'_{n,r}\right)\left(kf_r\prod_{m=1}^{N}\left[C_{m,r}\right]^{(\eta'_{m,r}+\eta''_{m,r})}\right) \tag{13}$$

$$\Gamma_{tb}=\sum_{m}^{N}\gamma_{m,r}C_{m,r} \tag{14}$$

$$kf_r=A_r T^{\beta_r}e^{\frac{-E_{a,r}}{RT}} \tag{15}$$

The ideal gas mixing law was used to compute the viscosity of the mixture. The viscosity of each species in the mixture was modeled by the Sutherland law. The specific heat of each species in Equation (10) was calculated as a function of the temperature via polynomials [59]. The mixture thermal conductivity required by the energy conservation equation was modeled according to Equation (16). The mass and thermal diffusion coefficients in Equation (8) were modeled according to Equations (17) and (18), respectively, whereas the turbulent diffusion coefficient was derived according to the turbulence models used [55, 56].

$$K=\sum_n\frac{X_n k_n}{\sum_m X_m\psi_{nm}} \tag{16}$$

$$D_n=\frac{1-n}{\sum_{n,m\neq n}(X_m/D_{nm})} \tag{17}$$

$$D_{T,n}=-2.59x10^{-7}T^{0.659}\left|\frac{M_{W,n}^{0.511}X_n}{\sum_{i=1}^{N}M_{W,n}^{0.511}X_n}-Y_n\right|\left|\frac{\sum_{n=1}^{N}M_{W,n}^{0.511}X_n}{\sum_{n=1}^{N}M_{W,n}^{0.489}X_n}\right| \tag{18}$$

The system of equations was solved numerically by the k-ε RNG turbulence model using the commercial software ANSYS Fluent to simulate the Borrows and Kurkov experiment [52]. In addition, the same system was solved by replacing the fluctuating terms with the SST k-ω turbulence model. For both turbulence models, two sets of reactions were analyzed: one with a 7-step reactions mechanism and one with an 18-step reaction mechanism, explained in section 2.1.3 and presented in the appendix. The system of equations was discretized by a control-volume-based technique. Second-order Upwind and least-squares cell-based schemes were used to discretize the convection and gradient terms, respectively. The density-based solver available in the ANSYS Fluent software was selected for the simulation [59].

2.1.2 Plasma Model

Experimental Intensified Charge-Coupled Device (ICCD) camera images of nanosecond-pulsed discharges in air and hydrogen [60, 61] have shown that plasma is generated in an approximately rectangular, narrow shape near the lower wall, in the volume between the electrodes. In addition, it has been shown that the plasma is nearly uniform during each pulse. Starikovskaia et al. [62] also confirmed the uniformity of nanosecond-pulsed discharges in a gas mixture between 0.3 and 2.4 atm. Kosarev et al. [63] discussed the ability of these types of discharges to generate a quasi-uniform plasma layer behind a shock wave from a shock tube. As a result of these findings, certain studies for supersonic hydrogen-air mixtures [42, 51] have proposed modeling the plasma in a volumetric constant region with a uniform electric field throughout the domain. This approach reduces the computational load imposed by solving Poisson's equation when computing electric fields and is utilized in this work to uniformly model the production of plasma active species in a constant volume between discharge electrodes. This is done by using a constant electric field derived from the discharge parameters.

Due to the spatial uniformity of the plasma model in this work, the number density of the species produced during each pulse of the discharge is only a function of time. Thus, by eliminating the spatial transport term in equation (19), it is not necessary to solve the highly computationally-demanding electric potential equation. In addition, the current modeling approach does not consider the calculation of ion Joule heating because the energy contribution of this phenomenon is rapidly dissipated by convection. Finally, compared to electric fields, the current densities and induced magnetic fields are thought to have a minor impact on plasma physics of the nanosecond pulsed discharge [43].

$$\frac{\partial n_k}{\partial t} + \nabla \cdot \Gamma_k = \dot{G}_k, \quad k = 1, 2, 3 \tag{19}$$

As a result of the aforementioned assumptions, the plasma modeling approach used in this work calculates the concentrations of species generated during the application of an electric discharge solely as a function of time as shown in equation (20). This gives way to a system of nonlinear ordinary differential equations as shown in equations (21), (22) and (23), saving computational resources while still capturing its main effects.

$$\frac{dn_k}{dt} = \sum_{m=1}^{m} Q_{km}(t) \tag{20}$$

$$aA + bB \rightarrow a'A + cC \tag{21}$$

$$Rp_m = kp_m[A]^a[B]^b \tag{22}$$

$$Q_A = (a' - a)Rp_m; \;\; Q_B = -bRp_m; \;\; Q_c = cRp_m \tag{23}$$

The first step in calculating the plasma species concentration is to define an appropriate plasma reaction mechanism that includes all the processes that occur during the discharge. This work follows the approach used by Kosarev et al. [63], in which the production of plasma species is focused on those reactions that lead to the dissociation of the initial species in the mixture. In this manner, radicals can be generated and subsequently become involved in the ignition process.

Dissociation can occur directly as a result of electron-impact dissociation or indirectly as a result of different reactions between excited species produced by electron impacts. Therefore, electron dissociation, attachment, detachment, excitation, and ionization, as well as excited species quenching, charge exchange and electron-ion recombination processes, are considered in the plasma kinetic mechanism described as in equation (21). The rates of each of these reactions, kp, must then be calculated as a function of the electron energy distribution, which is derived from the solution of the Boltzmann equation.

To solve the Boltzmann equation, the freeware Bolsig+ [54] was utilized. The software numerically calculates the electron energy distribution function. The required inputs are the thermodynamic gas properties, the gas composition, the reduced electric field of the plasma and the collision cross-sections of the processes that occur during the discharge.

An important task in solving the Boltzmann equation that was assisted by Bolsig+ was determining the correct collision processes that apply to the plasma reactions that need to be modeled. For each collision process of the model, information about the corresponding cross-section is required.

The rate coefficients calculated from Bolsig+ were used by a plasma kinetic solver to determine the time evolution of the species produced during discharge. This plasma solver is named ZDPlaskin [53], and it is a Fortran 90 module that calculates the kinetics of a plasma discharge in time for any gas mixture. ZDPlaskin includes Bolsig+. As a result, all the electric discharge information required by Bolsig+ is added as input to ZDPlaskin, and the electron-impact reaction rates are calculated internally by Bolsig+.

The time evolution of the species densities was expressed as a system of ordinary differential equations (ODEs), which was formed by the set of production/consumption rates of the species involved in the plasma kinetic mechanism. In ZDPlaskin, the time evolution of the plasma species was obtained by integration using the solver DVODE F90 [64].

2.1.3 Chemistry

For the model presented in this work, H_2-air mixtures were defined in the laminar finite rate model. The net source of the chemical species was calculated by dividing the sum of the Arrhenius reaction sources by the total number of reactions involved. In this work, two sets of , H_2-air chemical reactions were included in the model: a set of 7 reactions developed by Jachimowski [65] and modified by Eklund et al. [57] and a set of 18 reactions from [58].

Since the electrical discharge in this work was applied in, H_2-air, a plasma kinetics reaction mechanism of 133 reactions involving these gases was utilized. To model radical generation, information on O_2 dissociation, ionization and excitation reactions, as well as their cross sections, were taken from [66]. This was done so that their rate coefficients could be calculated via Bolsig+. Likewise, the information required for, H_2 dissociation, ionization and excitation reactions was taken from [67]. Most of the reactions in the mechanism are related to N_2 species. It can also be seen from [68] that electron-ion recombination and positive ion recombination reactions generate O radicals from Nitrogen derived species produced by the remaining mechanism reactions.

3. Simulation Configuration

3.1 Flow Conditions

In this work, a nanosecond-pulsed electric discharge was applied to the domain of the backward-facing step experiment of Burrows and Kurkov [52], following the proposed methodology. The experiment of Burrows and Kurkov involved a supersonic combustor with sonic injection of hydrogen fuel from a backward-facing step parallel to a high-temperature supersonic-vitiated free stream air flow generated by burning a hydrogen-nitrogen mixture with high-pressure liquid oxygen, as shown in Figure 2. According to Burrows and Kurkov, the good heat-sink capacity of the chamber and the short duration of the experiment allowed for the modeling of a 298 K constant temperature in the wall. Table 1 summarizes the flow conditions of the experiment. It is worth noting that the experiment did not include the application of an electric discharge when it was performed. Therefore, the current work is novel in that it computationally applies plasma to the original experiment and studies the effects of the discharge on the combustion process.

Table 1. Experimental Flow Conditions.

Property	Air	Fuel
Mach Number	2.44	1.0
Static Temperature (K)	1270	254
Static Pressure (kPa)	101.325	101.325
H_2 Mass Fraction	0.0	1.0
O_2 Mass Fraction	0.258	0.0
N_2 Mass Fraction	0.486	0.0
H_2O Mass Fraction	0.256	0.0

The grid that was used is shown in Figure 3. It has 22916 elements and was refined near the injector, the wall above the injector where a shear layer developed in the x-direction, and at the combustor entrance where Mach waves were expected. The grid was also refined near the walls to capture the boundary layer effects, as recommended in [69]. For the construction of the mesh and the configuration of the simulations the lowest distance in the mesh was about 4 x 10^{-5} m. This criterion was stablished to achieve a courant number less than one with time step value of 1.2 x 10^{-8} s in the temporal simulation when the plasma was applied.

Boundary conditions were imposed according to the flow conditions shown in Table 1. Pressure boundary conditions for the air and fuel inlets were established by specifying pressures, temperatures and Mach numbers. The constant-temperature wall condition of 298 K suggested by Burrows and Kurkov was assumed in conjunction with the nonslip condition for velocity.

Four test cases were run to verify that the selected compressible-turbulence-reacting flow model, mesh, boundary conditions and numerical procedures were adequate for simulating the physical phenomena. These test cases resulted from the combination of the two turbulence models with the two reaction mechanisms. Results from these test cases were validated against the experimental data of the work of Burrows and Kurkov provided in [69].

The simulations were performed via Ansys Fluent using a coupled implicit solver with Second Order Upwinding and Quick schemes for discretization of transport equations. Residuals of mass, momentum, energy, turbulence variables and species conservations reached minimum order of 10^{-4}.

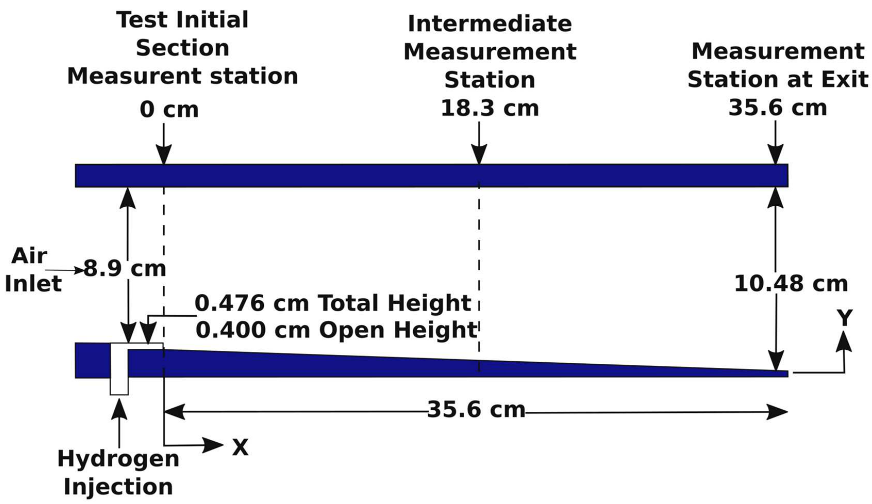

Fig. 2. Schematic of the backward-facing step combustor used in Ref. [52].

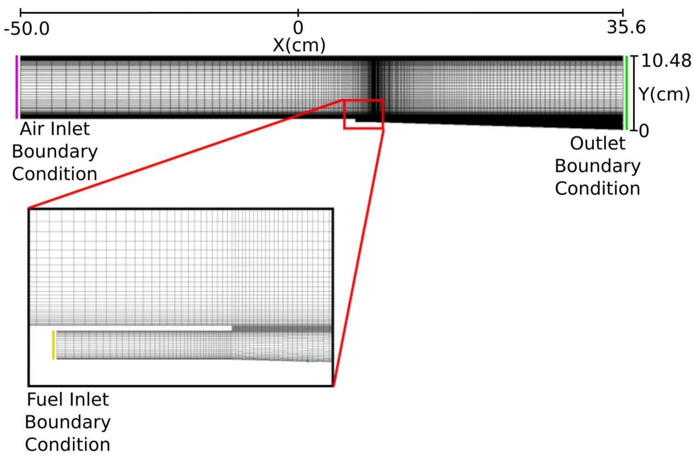

Fig. 3. Computational mesh.

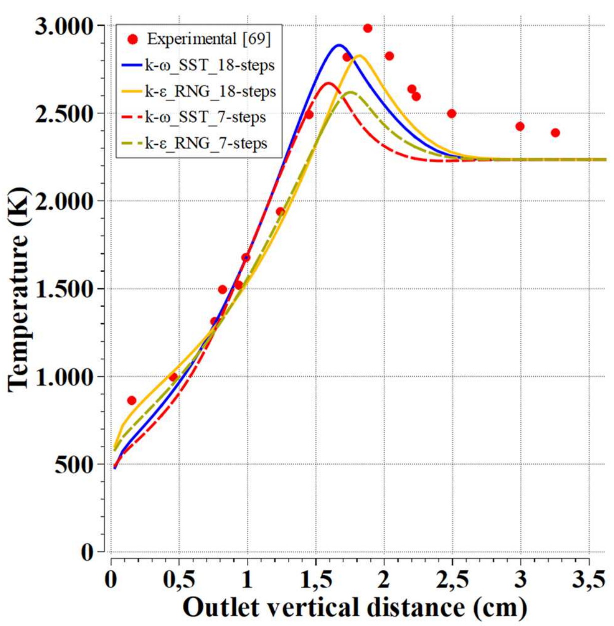

Fig. 4. Total temperature at the backward-facing step exit port.

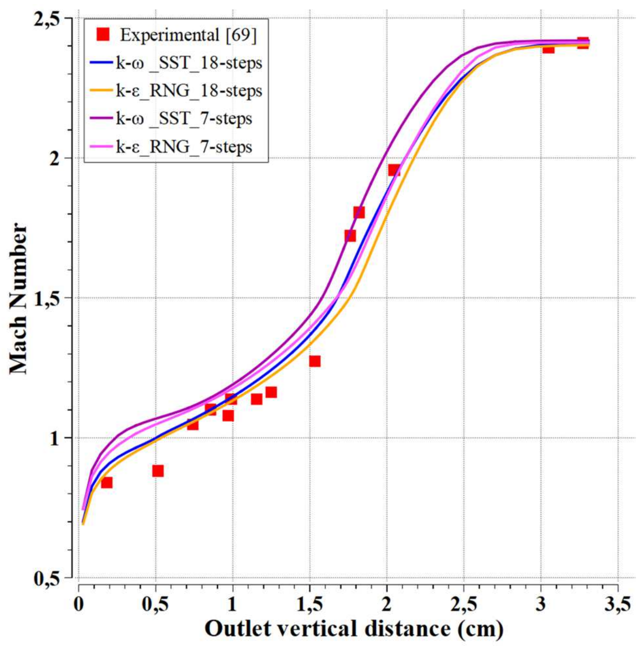

Fig. 5. Mach number at the backward-facing step exit port.

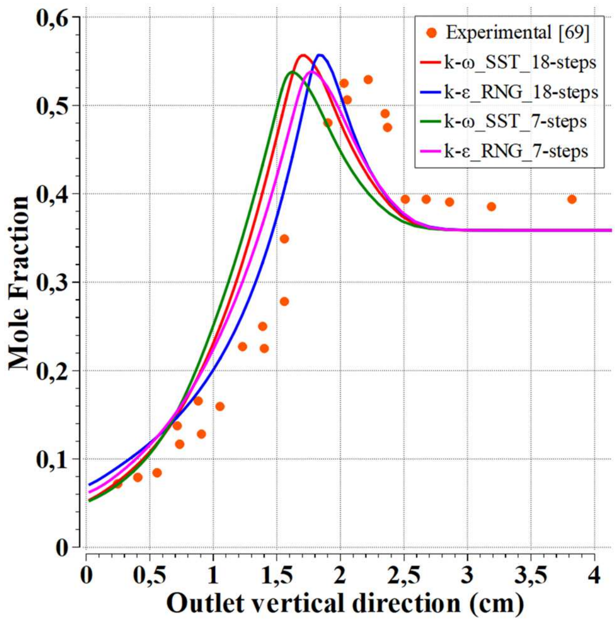

Fig. 6. H_2O mole fraction at the backward-facing step exit port.

As shown in Figure 4, 5 and 6, simulations with an 18-step mechanism had lower relative errors than simulations with a 7-step mechanism for temperature, Mach number and water vapor mole fraction profiles at the exit of the combustor, vertical direction, confirming the importance of the additional species. Relative errors of 6.17 % and 4.94% for temperature and Mach number profiles, respectively Figures 4 and 5, at the exit of the combustor were obtained with the 18-step mechanism. While the 7-step mechanism has a lower computational cost than simulations with a greater number of reactions and species, the 18-step mechanism includes species such as HO_2.

Jachimowski [65], Mattick and Frankel [70] and Evans et al. [71] revealed the significance of the HO_2 species in autoignition prediction in high-speed flow combustion. In fact, HO_2 species provide adequate reaction paths for generating radicals that promote combustion, such as OH. The absence of this critical species may lead to an underestimation of the flame temperature. In addition, the results show that the k-ε RNG model with the 18-step mechanism has the lowest relative errors to the experimental data for total temperature and species mole fraction, while the SST k-ω model with 18 steps has the lowest relative error for Mach number data.

Due to the results of the previous simulations, the k-ε RNG turbulence model with the 18-step mechanism was established to implement the proposed methodology and simulate the application of nanosecond-pulsed discharges in the experiment of Burrows and Kurkov [52].

Table 2. Different cases run for the backward-facing step combustor configuration.

Case	Label	T (K)	Plasma Region
1	NPAC	1270	-
2	PACR1	1270	1
3	PACR2	1270	2
4	LNPAC	1200	-
5	LPACR2	1200	2

3.2 Nanosecond Pulsed Discharge Conditions

As a result, five different simulation cases were used to study the PAC phenomena on the backward-facing step configuration, as shown in Table 2. All cases used the same numerical approach, domain, mesh and flow conditions as in the previous simulations. The cases differ in terms of the incoming air temperature and the region where the discharge was applied. Case number 1, labeled NPAC, was set with the same flow conditions as the previous simulation and is shown in Table 1 without the plasma applied. Case numbers 2 and 3, labeled PACR1 and PACR2, respectively, were used to assess the ability of the proposed PAC methodology to reduce the ignition delay time. This was accomplished by applying the nanosecond-pulsed discharge at two different locations along the combustor. The first location was labeled Plasma Region 1 and was set between 0.05 and 0.07 m from the origin of the computational domain in the x-direction. Case number 2, PACR1, corresponds to the application of the plasma in this region. The second location, labeled Plasma Region 2, was set between 0.09 and 0.11 m from the origin in the x-direction. Case number 3, PACR2, corresponds to this region. The locations of these regions inside the numerical domain are shown in Figure 7. The purpose on selecting these locations was to explore the effect of the plasma when the discharge region is moved downstream. The flow conditions for these cases were identical to those in Table 1.

Cases 4 and 5, labeled LNPAC and LPACR2, respectively, were established with similar flow conditions to the previously presented cases but at a lower air temperature. The goal of simulating these two cases was to evaluate the influence of the discharge when the temperature of the incoming air was too low to cause autoignition. For this purpose, the air temperature in the previous simulations shown in Table 1, 1270 K, was lowered to 1200 K. When the case with this lower temperature was run without plasma application, no flame was observed inside the computational domain. As a result, this temperature was selected to evaluate the capability of the proposed PAC model to enhance combustion under this particular condition. Case number 4, LNPAC, was simulated in the absence of plasma discharge, whereas case number 5, LPACR2, was simulated with plasma discharge applied in plasma region 2, as shown in Table 2.

The nanosecond pulsed discharge utilized in the simulation was reproduced from that implemented in the experiment performed by Do [49]. As a result, all the information concerning the plasma discharge was taken from that study. The reduced electric field of the pulsed discharge was estimated to be 300 Td, 10 ns pulse width and 50 kHz repetition rate according to the discharge conditions: repetitive 15 kV peak pulses, 300 K and 6 mm electrode separation. An approximate nominal power of 10 W was consumed between the plasma pulses. That is, each 20 µs. The energy of a pulse was about 0.2 mJ. The initial electron density was set to 10^{18} m^{-3}. The information of this reduced electric field was utilized by the zero-dimensional plasma solver ZDPlaskin to calculate the reaction rate constants and subsequently, the temporal evolution of the species. This, via the solution of the Boltzmann equation.

4. Results and Discussion

4.1 Reduction of the Ignition Delay Time

The time sequential temperature contours presented in Figure 8 show the effect of the presented plasma modeling approach on the backward-facing step flame via reduction of the ignition delay time of the mixture. The left column of the figure shows case number 1, NPAC, for which no plasma discharge was applied and typical supersonic combustion occurs. The right column displays case number 3, PACR2, which had a flame after an electric discharge was applied.

Three main differences can be observed in Figure 8 by comparing case number 1 and case number 3. First, at 60 µs, ignition occurred, and a stable flame was formed when plasma was applied in case number 3, PACR2. Conversely, no ignition was observed when there was no plasma discharge applied in case number 1, NPAC, indicating that the ignition delay time has been shortened due to the electric discharge. Second, at 90 µs, only a slight rise in temperature was observed for the NPAC case. In contrast, for the PACR2 case, at 90 µs, the flame has already reached the combustor outlet. In fact, the flame propagates faster downstream of the combustor when plasma is applied, which is also a consequence of the earlier ignition process. Finally, at 120 µs, the flame in the NPAC case has propagated toward the end of the domain. Nonetheless, it was thinner than the flame formed in the PACR2 case when plasma was applied.

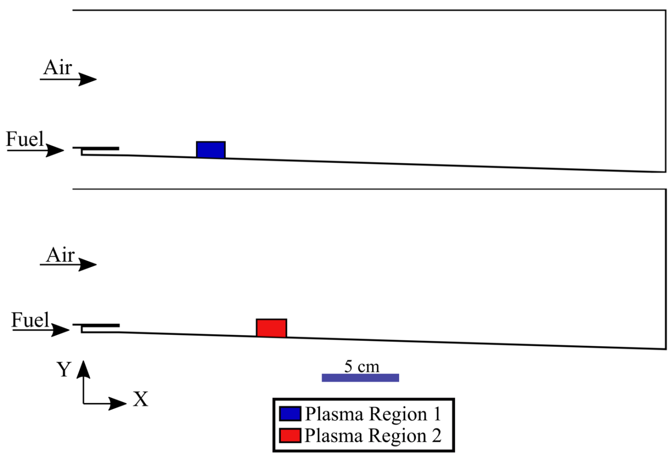

Fig. 7. Plasma regions inside the numerical domain.

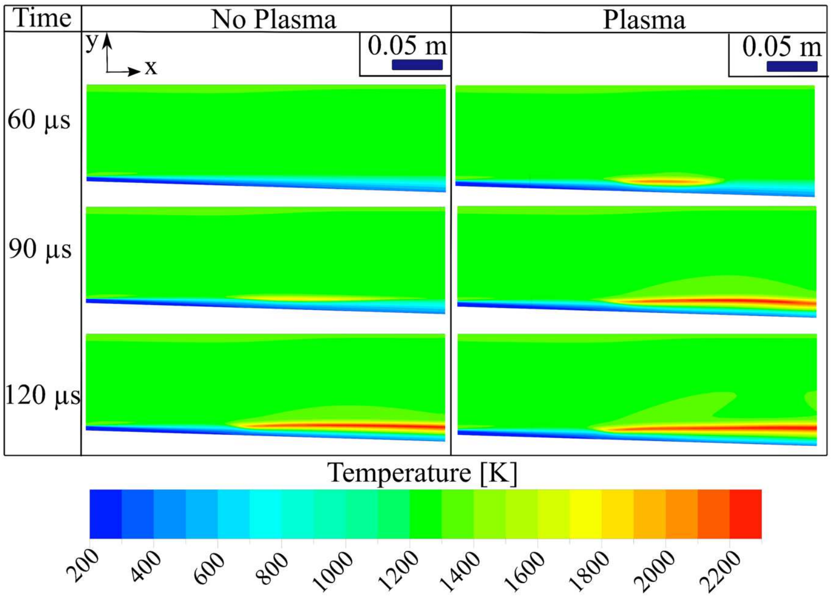

Fig. 8. Time evolution showing the contours of static temperature at 60, 90 and 120 μs for the backward-facing step configuration for case number 1, NPAC (left column) and case number 3, PACR2 (right column).

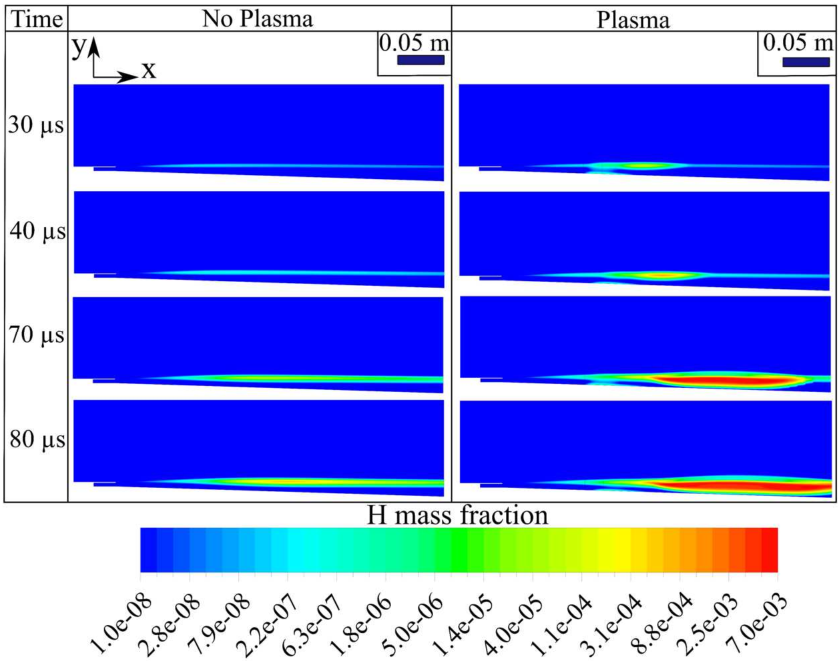

Fig. 9. Time evolution showing the contours of the H mass fraction at 30, 40, 70 and 80 μs for the backward-facing step configuration for case number 1, NPAC (left column) and case number 3, PACR2 (right column).

The reduction in ignition delay time when plasma is applied, as in the PACR2 case, can be explained by the seeding effect of the O and H radicals on the combustion simulation used in the proposed methodology, as shown in Figure 9. This figure shows the time evolution of the contours of the H radical mass fraction. The left column displays the results for case number 1, NPAC, and the right column displays the results for case number 3, PACR2. This figure shows the seeding and convection of H radicals in the discharge region as a result of plasma application. According to the combustion mechanism used in these simulations, which was presented in [58], chain initiation reactions 1 and 2 have the highest activation energies in the entire mechanism and therefore require higher temperature to accelerate. Nonetheless, OH and O radicals resulting from these reactions lead to an exponential increase in the concentration of O, H and OH radicals through faster reactions 3, 4, 11 and 12, promoting ignition. As a result, the ignition delay time is controlled by reactions 1 and 2 because they are the slowest. This process occurs in the NPAC case. In the PACR2 case, on the other hand, the plasma seeding of O and H radicals (shown for H radicals in Figure 9) bypasses the slowest reactions 1 and 2, providing radicals that participate in branching reactions 4, 8, 11 and 12, resulting in a faster exponential increase of radicals than in the NPAC case. As a result, the ignition delay time is reduced. This faster increase in H radicals, shown in the right column of Figure 9 for the PACR2 case, causes ignition to occur earlier, as shown in Figure 8.

Finally, the results in Figure 9 show that the proposed PAC simulation methodology for supersonic flows in this work, which adopts the combustion mechanism in [58], is capable of capturing the nanosecond-pulsed discharge effects in shortening the ignition delay time for the backward-step combustor.

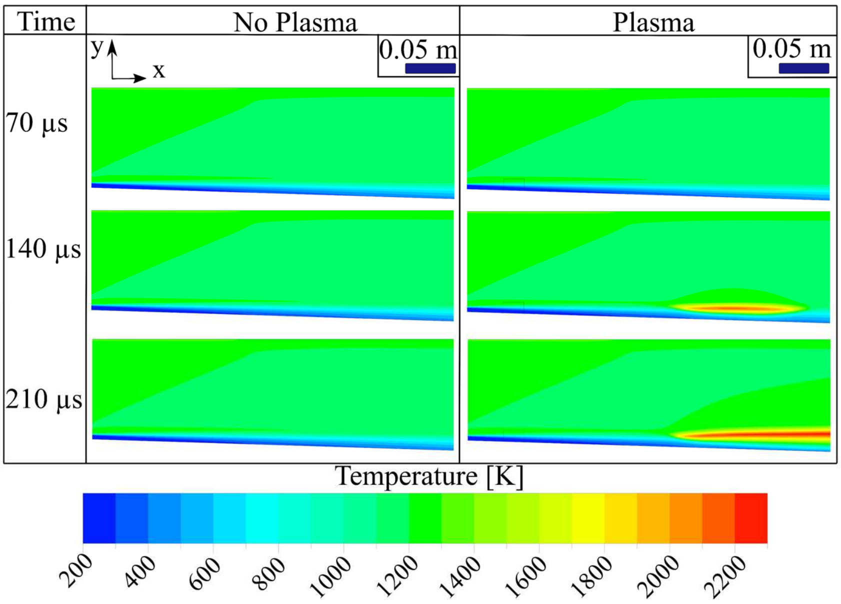

Fig. 10. Time evolution of the static temperature contours at the backward-facing step for the LNPAC (left column) and LPACR2 cases (right column).

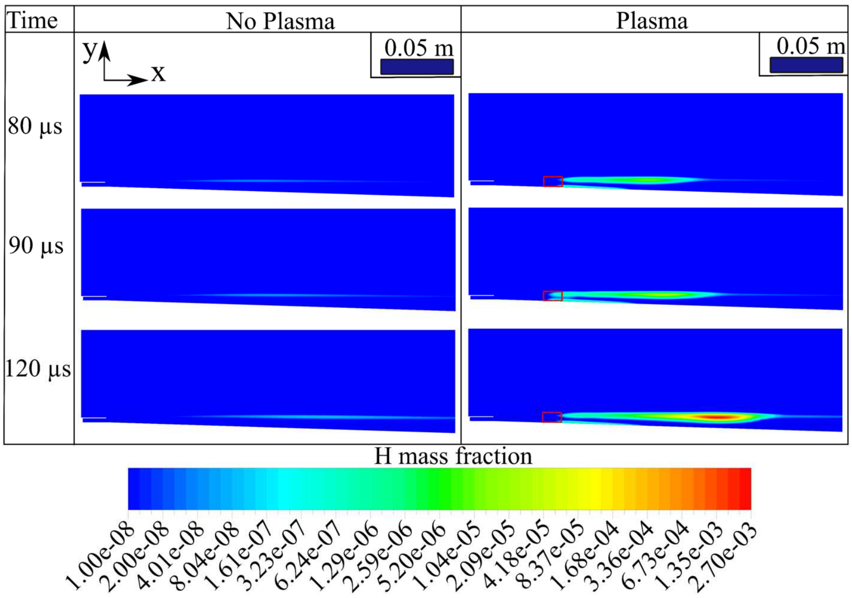

Fig. 11. Time evolution of the H mass fraction contours at the backward-facing step for the LNPAC (left column) and LPACR2 cases (right column).

4.2 Low-enthalpy Flow Condition Plasma Enhancement

Figure 10 compares the time sequential temperature contours of case number 4, LNPAC, in the left column, to case number 5, LPACR2, in the right column, in which a nanosecond pulsed discharge was applied. The contours in the left column show that no ignition occurred in the absence of plasma. On the other hand, the right column indicates that when plasma was applied, a flame appeared approximately at 140 μs, and at 210 μs, this flame reached the combustor outlet.

The air temperature in the LNPAC case was insufficient to accelerate reactions 1 and 2 from the reaction mechanism in [58] before the high-speed flow convected the mixture out of the domain. Therefore, not enough radicals were generated to trigger ignition. In the LPACR2 case, on the other hand, the plasma-seeded radicals allowed reactions 1 and 2 to be bypassed, accelerating the chain branching process to compensate for the high-speed transport, generating enough radicals to induce ignition. This increase in the production of radicals when plasma is applied is illustrated in Figure 11. This figure displays the time evolution contours of the H radical mass fraction for the LNPAC case in the left column and for the LPACR2 case in the right column. Figure 11 shows that the amount of H radicals generated in the LPACR2 case (when plasma was applied) was significantly greater than that in the LNPAC case as time evolved, confirming that the radicals produced in the LNPAC case were insufficient to trigger ignition and induce a flame.

5. Conclusions

In this work, a reduced-order modeling approach for plasma-assisted combustion of Hydrogen/air mixtures at supersonic speeds was presented, allowing the principal effects of nonequilibrium electric discharges in scramjet engines to be evaluated. This approach is unique in that it couples a zero-dimensional plasma model to a flow combustion model that includes thermal and mass diffusion, finite rate chemistry, and turbulence and compressibility effects, whereas previous approaches have considered either zero-dimensional plasma models with flow models that neglect compressibility, turbulence and mixing effects or highly-detailed plasma models with complete CFD combustion models. In order to determine the performance of the current approach different simulations were carried out. Two combustion reaction mechanisms involving O and H radicals showed to be capable of reproducing experimental detailed data from supersonic combustion. Similarly, the proposed reduced plasma-flow couple approach demonstrated its capability in capturing the nanosecond pulsed discharge effects on supersonic combustion through the simulation of two different configurations of combustors.

The simulation results for the application of the nanosecond-pulsed discharge on the backward-facing step combustor showed that the ignition delay time was lower than in the cases when no discharge was applied. This is a clear result of the capability of the proposed approach. The implemented plasma model provides sufficient O and H radical concentrations that interact with the air and fuel mixture, according to the selected 18-step combustion reaction mechanism. The introduction of these radicals allowed the slowest reactions of the mechanism in [58] to be bypassed, resulting in shorter ignition delay times.

Simulations of the case with an air flow at 1200 K with no ignition showed that the application of a plasma discharge causes a flame to appear inside the combustor. At this temperature, reactions 1 and 2 in [58] were unable to initiate chain branching and ignition before the mixture left the domain due to their high activation energies. The introduction of plasma radicals O and H solve this problem by bypassing these reactions, reducing the ignition delay time and allowing the mixture to ignite inside the combustor despite the high convection effects of the flow.

These results confirm that the proposed modeling approach can capture and reproduce the effects of plasma discharge in supersonic combustion, which can be further investigated in future work.

Author Contributions

L.F. Alvarez and A.D. Gutierrez developed the methodological approach, including the computational frame, designed the simulation strategy, examined the theory validation utilizing previous experiments and analyzed the numerical results; L.F. Alvarez conducted the simulations. The manuscript was written through the contribution of all authors. All authors discussed the results, reviewed, and approved the final version of the manuscript.

Acknowledgments

This work was supported by the Universidad del Valle.

Conflict of Interest

The authors declared no potential conflicts of interest concerning the research, authorship, and publication of this article.

Funding

The authors received no financial support for the research, authorship, and publication of this article.

Data Availability Statements

The datasets generated and/or analyzed during the current study are available from the corresponding author on reasonable request.

Nomenclature

A_r	Pre-exponential factor, m, kmol, s^{-1}
β_r	Temperature exponent
$C_{m,r}$	Molar concentration of species m in reaction r, kmol m^{-3}
$c_{p,n}$	Specific heat capacity at constant pressure of species n, J kg^{-1} K^{-1}
$D_{T,n}$	Thermal diffusion of species n, kg m^{-1} s^{-1}
D_n	Mass diffusion coefficient for species n in the mixture, m^2 s^{-1}
$D_{n,m}$	Binary diffusion of species n in each species m, m^2 s^{-1}
$\tilde{e}$	Favre-averaged internal energy, J Kg^{-1}
E	Total energy, J Kg^{-1}
$E_{a,r}$	Activation energy for reaction r, J kmol^{-1}
$\dot{G}_k$	Plasma species k generation/destruction term, m^{-3} s^{-1}
h	Enthalpy of the mixture, J kg^{-1}
h_n	Sensible enthalpy of species n, J kg^{-1}
$\tilde{h}$	Favre-averaged enthalpy, J kg-1
h''	Fluctuating-Favre enthalpy, J kg-1
H	Total enthalpy, J kg^{-1}
$J_{n,j}$	Diffusion flux of species n in direction j, kg m^{-2} s^{-1}
K	Thermal conductivity of the mixture, W m^{-1} K^{-1}
K_n	Thermal conductivity of the species n, W m^{-1} K^{-1}
k	Turbulence kinetic energy, m^2 s^{-2}
kf_r	Forward rate constant for reaction r, kmol m^{-3} s^{-1}, s^{-1}, m^3 mol^{-1} s^{-1}
$\mathcal{M}_n$	Symbol denoting species n
$M_{W,n}$	Molecular weight of species n, kg kmol^{-1}
N	Total number of chemical species in the system
N_R	Total number of reactions in the system
n_k	Number density of plasma species k, m^{-3}
$\bar{P}$	Reynolds-averaged static pressure, kg m^{-1} s^{-2}
P_{op}	Operating pressure, J kmol^{-1} K^{-1}
Q_{km}	Source terms for the species k corresponding to the contributions from different plasma reactions m, m^{-3} s^{-1}

R Universal gas constant, J kmol^{-1} K^{-1}
R_n Net rate of production of species n by chemical reactions, kg m^{-3} s^{-1}
$\widehat{R_{n,r}}$ Arrhenius molar rate of creation/destruction of species n in reaction r, kmol m^{-3} s^{-1}
Rp_m Reaction rate of plasma species m, m^{-3} s^{-1}
S_h Volumetric heat source, J Kg^{-1}s^{-1}
Sc_t Turbulent Schmidt number
t Time, s
T Favre-averaged temperature, K
$\tilde{T}$ Favre-averaged temperature, K
T_{ref} Reference temperature, K
$\tilde{u_i}$ Favre-averaged velocity vector in i direction, m s^{-1}
u_i'' Fluctuating-Favre velocity vector in i direction, m s^{-1}
$\tilde{u_j}$ Favre-averaged velocity vector in j direction, m s^{-1}
u_j'' Fluctuating-Favre velocity vector in j direction, m s^{-1}
$v'_{n,r}$ Stoichiometry coefficient for reactant n in reaction r
$v''_{n,r}$ Stoichiometry coefficient for product n in reaction r
x_p Distance in p direction
x_q Distance in q direction
X_n Mole fraction of species n
X_m Mole fraction of species m
Y_n Local mass fraction of species n

Greek symbols

Γ_k Species k flux number, m^{-1} s^{-1}
Γ_{tb} Net effect of third bodies on the reaction rate, mol m^{-3}
$\gamma_{m,r}$ Third body efficiency of the mth species in the r th reaction
$\eta'_{n,r}$ Rate exponent for reactant species n in reaction r
$\eta''_{n,r}$ Rate exponent for product species n in reaction r
μ_t Turbulent dynamic viscosity, kg m^{-1} s^{-1}
$\bar{\rho}$ Reynolds-averaged density, kg m^{-3}
$\bar{\tau}$ Averaged viscous shear stress tensor, kg m^{-1} s^{-2}
ψ_{nm} Function of the properties of pure components of the mixture

Subscripts

a Activation
mix Mixture
m Species m
n Species n
op Operating
p Direction p
q Direction q
R Total reactions
r Reaction rth
ref Reference
tb Third body

Appendix

Reaction mechanisms:

Table A-1. 7-step combustion reaction mechanism [57].

Number	***Reaction***	A_r (cm, kmol, s)	β_r	$E_{a,r}\,R^{-1}$ (K)
$R1$	$H_2 + O_2 \rightarrow OH + OH$	1.70×10^{13}	0.0	24245
$R2$	$H + O_2 \rightarrow OH + O$	1.42×10^{14}	0.0	8258
$R3$	$OH + H_2 \rightarrow H_2O + H$	3.16×10^{7}	1.8	1525
$R4$	$O + H_2 \rightarrow OH + H$	2.07×10^{14}	0.0	6923
$R5$	$OH + OH \rightarrow OH + OH$	5.50×10^{13}	0.0	3525
$R6$	$H_2 + O_2 \rightarrow H_2O + M_1$	2.21×10^{22}	-2.0	0
$R7$	$H + H \rightarrow H_2 + M_2$	6.53×10^{17}	-1.0	0

Table A-2. 18-step combustion reaction mechanism [58].

Number	***Reaction***	A_r (cm, kmol, s)	β_r	$E_{a,r}\,R^{-1}$ (K)
$R1$	$H_2 + O_2 \rightarrow OH + OH$	1.70×10^{13}	0.0	24230
$R2$	$H + O_2 \rightarrow OH + O$	2.00×10^{14}	0.0	8455
$R3$	$OH + H_2 \rightarrow H_2O + H$	1.00×10^{8}	1.6	1660.8
$R4$	$O + H_2 \rightarrow OH + H$	5.06×10^{14}	2.67	3163.1
$R5$	$OH + OH \rightarrow O + H_2O$	1.50×10^{9}	1.14	50.33
$R6$	$H + OH + M \rightarrow H_2O + M$	2.22×10^{22}	-2.0	0.0
$R7$	$H + H + M \rightarrow H_2 + M$	1.80×10^{18}	-1.0	0.0
$R8$	$H + O_2 + M \rightarrow HO_2 + M$	2.30×10^{18}	-0.8	0.0
$R9$	$HO_2 + OH \rightarrow H_2O + O_2$	6.00×10^{13}	0.0	0.0
$R10$	$HO_2 + H \rightarrow H_2 + O_2$	2.53×10^{13}	0.0	352.3
$R11$	$HO_2 + H \rightarrow OH + OH$	1.50×10^{14}	0.0	505.28
$R12$	$HO_2 + O \rightarrow OH + O_2$	1.80×10^{13}	0.0	-203.8
$R13$	$O + O + M \rightarrow O_2 + M$	2.90×10^{17}	-1.0	0.0
$R14$	$HO_2 + H \rightarrow H_2O + O$	3.00×10^{13}	0.0	865.63
$R15$	$HO_2 + HO_2 \rightarrow H_2O_2 + O_2$	2.50×10^{11}	0.0	-626.57
$R16$	$OH + OH + M \rightarrow H_2O_2 + M$	3.25×10^{22}	-2.0	0.0
$R17$	$H_2O_2 + H \rightarrow H_2O + OH$	1.00×10^{13}	0.0	1804.2
$R18$	$H_2O_2 + OH \rightarrow H_2O + HO_2$	5.40×10^{12}	0.0	505.26

References

[1] Corin, S., The Scramjet Engine: *Processes and Characteristics*, *Cambridge University Press*, Cambridge, 2009.
[2] Jazra, T., Preller, D., Smart, M.K., Design of an Airbreathing Second Stage for a Rocket-Scramjet-Rocket Launch Vehicle, *Journal of Spacecraft and Rockets*, 50(2), 2013, 411–422.

[3] Kanda, T., Kudo, K., Payload to Low Earth Orbit by Aerospace Plane with Scramjet Engine, *Journal of Propulsion and Power*, 13(1), 1997, 164–166.
[4] Preller, D., Smart, M.K., Reusable Launch of Small Satellites Using Scramjets, *Journal of Spacecraft and Rockets*, 54(6), 2017, 1317–1329.
[5] Smart, M.K. Tetlow, M.R., Orbital Delivery of Small Payloads Using Hypersonic Airbreathing Propulsion, *Journal of Spacecraft and Rockets*, 46(1), 2009, 117–125.
[6] Tetlow, M.R., Doolan, C.J., Comparison of Hydrogen and Hydrocarbon-Fueled Scramjet Engines for Orbital Insertion, *Journal of Spacecraft and Rockets*, 44(2), 2007, 365–373.
[7] Fuhs, A., Future Science and Technology for Military Space, American Institute of Aeronautics and Astronautics, *Space Programs and Technologies Conference, Huntsville*, AL, U.S.A., 1990.
[8] Conner, M., NASA Flights to Examine Improved Supersonic Flight Efficiency, NASA, 2017. http://www.nasa.gov/centers/armstrong/features/swept_wing_laminar_flow_test.html (accessed October 20, 2021).
[9] Mitani, T., Ignition Problems in Scramjet Testing, *Combustion and Flame*, 101(3), 1995, 347–359.
[10] Tian, Y., Yang, S., Xiao, B., Zhong, F., Le, J., Investigation of Ignition Characteristics in a Kerosene Fueled Supersonic Combustor, *Acta Astronautica*, 161, 2019, 425–429.
[11] Scheuermann, T., Chun, J., Von Wolfersdorf, J., Experimental Investigations of Scramjet Combustor Characteristics, *AIAA International Space Planes and Hypersonic Systems and Technologies Conference*, Dayton, Ohio, U.S.A., 2008.
[12] Gaston, M., Mudford, N., Houwing, F., A comparison of Two Hypermixing Fuel Injectors in a Supersonic Combustor, American Institute of Aeronautics and Astronautics, 36th AIAA Aerospace Sciences Meeting and Exhibit, Reno, NV, U.S.A., 1998.
[13] Kodera, M., Sunami, T., Sheel, F., Numerical Study on the Supersonic Mixing Enhancement Using Streamwise Vortices, American Institute of Aeronautics and Astronautics, *AIAA/AAAF 11th International Space Planes and Hypersonic Systems and Technologies Conference*, Orleans, France, 2002.
[14] Ben-Yakar, A., Hanson, R., Supersonic Combustion of Cross-flow Jets and the Influence of Cavity Flame-holders, American Institute of Aeronautics and Astronautics, *37th Aerospace Sciences Meeting and Exhibit*, Reno, NV, U.S.A., 1999.
[15] McMillin, B.K., Seitzman, J.M., Hanson, R.K., Comparison of NO and OH Planar Fluorescence Temperature Measurements in Scramjet Model Flowfield, *AIAA Journal*, 32(10), 1994, 1945–1952.
[16] Correa, S., Warren, R., Supersonic Sudden-expansion Flow with Fluid Injection - An experimental and Computational Study, American Institute of Aeronautics and Astronautics, *27th Aerospace Sciences Meeting*, Reno, NV, U.S.A., 1989.
[17] Dutton, J., Herrin, J., Molezzi, M., Mathur, T., Smith, K., Recent Progress on High-speed Separated Base Flows, American Institute of Aeronautics and Astronautics, *33rd Aerospace Sciences Meeting and Exhibit*, Reno, NV, U.S.A., 1995.
[18] Fletcher, D., Mcdaniel, J., Quantitative Measurement of Transverse Injector and Free Stream Interaction in a Nonreacting SCRAMJET Combustor using Laser-induced Iodine Fluorescence, American Institute of Aeronautics and Astronautics, *25th AIAA Aerospace Sciences Meeting*, Reno, NV, U.S.A., 1987.
[19] Sato, N., Imamura, A., Shiba, S., Takahashi, S., Tsue, M., Kono, M., Advanced Mixing Control in Supersonic Airstream with a Wall-Mounted Cavity, *Journal of Propulsion and Power*, 15(2), 1999, 358–360.
[20] Yu, K. H., Schadow, K.C., Cavity-actuated Supersonic Mixing and Combustion Control, *Combustion and Flame*, 99(2), 1994, 295–301.
[21] Ben-Yakar, A., Hanson, R.K., Cavity Flame-Holders for Ignition and Flame Stabilization in Scramjets: An Overview, *Journal of Propulsion and Power*, 17(4), 2001, 869–877.
[22] Liu, Q., Baccarella, D., Lee, T., Hammack, S., Carter, C.D., Do, H., Influences of Inlet Geometry Modification on Scramjet Flow and Combustion Dynamics, *Journal of Propulsion and Power*, 33(5), 2017, 1179–1186.
[23] Heiser, W., Pratt, D., Daley, D. Mehta, U., *Hypersonic Airbreathing Propulsion*, AIAA Education Series, Washington DC, 1994.
[24] Ombrello, T., Won, S.H., Ju, Y., Williams, S., Flame Propagation Enhancement by Plasma Excitation of Oxygen. Part I: Effects of O_3, *Combustion and Flame*, 157(10), 2010, 1906–1915.
[25] Ombrello, T., Won, S.H., Ju, Y., Williams, S., Flame Propagation Enhancement by Plasma Excitation Of Oxygen. Part II: Effects of $O_2(a^1\Delta g)$, *Combustion and Flame*, 157(10), 2010, 1916–1928.
[26] Yin, Z., Adamovich, I.V., Lempert, W.R., OH Radical and Temperature Measurements During Ignition Of H2-Air Mixtures Excited by a Repetitively Pulsed Nanosecond Discharge, *Proceedings of the Combustion Institute*, 34(2), 2013, 3249–3258.
[27] Sun, W., Uddi, M., Won, S.H., Ombrello, T., Carter, C., Ju, Y., Kinetic Effects of Non-Equilibrium Plasma-Assisted Methane Oxidation on Diffusion Flame Extinction Limits, *Combustion and Flame*, 159(1), 2012, 221–229.
[28] Smirnov, V.V., Stelmakh, O.M., Fabelinsky, V.I., Kozlov, D.N., Starik, A.M., Titova, N.S., On the Influence of Electronically Excited Oxygen Molecules on Combustion of Hydrogen–Oxygen Mixture, *Journal of Physics D: Applied Physics*, 41, 2008, 192001.
[29] Mintusov, E., Serdyuchenko, A., Choi, I., Lempert, W.R., Adamovich, I.V., Mechanism of Plasma Assisted Oxidation and Ignition of Ethylene–Air Flows by a Repetitively Pulsed Nanosecond Discharge, *Proceedings of the Combustion Institute*, 32(2), 2009, 3181–3188.
[30] Brumfield, B., Sun, W., Wang, Y., Ju, Y., Wysocki, G., Dual Modulation Faraday Rotation Spectroscopy of HO_2 in a Flow Reactor, *Optics Letters*, 39(7), 2014, 1783–1786.
[31] Takita, K., Uemoto, T., Sato, T., Ju, Y., Masuya, G., Ohwaki, K., Ignition Characteristics of Plasma Torch for Hydrogen Jet in an Airstream, *Journal of Propulsion and Power*, 16(2), 2000, 227–233.
[32] Kimura, I., Aoki, H., Kato, M., The Use of a Plasma Jet for Flame Stabilization and Promotion of Combustion in Supersonic Air Flows, *Combustion and Flame*, 42, 1981, 297–305.
[33] Chen, D.C.C., Lawton, J., Weinberg, F.J., Augmenting Flames with Electric Discharges, *Symposium (International) on Combustion*, 10(1), 1965, 743–754.
[34] Haselfoot, C.E., Kirkby, P.J., XLV. The Electrical Effects Produced by the Explosion of Hydrogen and Oxygen, *The London, Edinburgh, and Dublin Philosophical Magazine and Journal of Science*, 8(46), 2009, 471-481.
[35] Kobayashi, K., Mitani, T., Tomioka, S., Supersonic Flow Ignition by Plasma Torch and H_2/O_2 Torch, *Journal of Propulsion and Power*, 20(2), 2004, 294–301.
[36] Bradley, D., Ibrahim, S.M.A., Electron Temperatures in Flame Gases: Experiment and Theory, *Combustion and Flame*, 24, 1975, 169–171.
[37] Jaggers, H.C., Von Engel, A., The Effect of Electric Fields on the Burning Velocity of Various Flames, *Combustion and Flame*, 16(3), 1971, 275–285.
[38] Won, S.H., Ryu, S.K., Kim, M.K., Cha, M.S., Chung, S.H., Effect of Electric Fields on the Propagation Speed of Tribrachial Flames in Coflow Jets, *Combustion and Flame*, 152(4), 2008, 496–506.
[39] Do, H., Cappelli, M., Mungal, G., Plasma Assisted Cavity Flame Ignition in Supersonic Flows, *Combustion and Flame*, 157(9), 2010, 1783–1794.
[40] Voland, R., Rock, K., NASP Concept Demonstration Engine and Subscale Parametric Engine tests, American Institute of Aeronautics and Astronautics, *International Aerospace Planes and Hypersonics Technologies*, Chattanooga, TN, U.S.A, 2012.
[41] Breden, D., Raja, L., Simulations of Nanosecond Pulsed Plasmas in Supersonic Flows for Combustion Applications, *AIAA Journal*, 50(3), 2012, 647–658.
[42] Nagaraja, S., Multi-Scale Modeling of Nanosecond Plasma Assisted Combustion, Ph. D. Thesis, School of Aerospace Engineering, Georgia Institute of Technology, Atlanta, GA, 2014.
[43] Breden, D.P., Simulations of Atmospheric Pressure Plasma Discharges, Ph. D. Thesis, Department of Aerospace Engineering, The University of Texas at Austin, Austin, TX, 2013.
[44] Ju, Y., Sun, W., Plasma Assisted Combustion: Dynamics and Chemistry, *Progress in Energy and Combustion Science*, 48, 2015, 21–83.
[45] Castela, M.L., Fiorina, B., Coussement, A., Gicquel, O., Darabiha, N., Laux, C., Modelling the Impact of Non-Equilibrium Discharges on Reactive Mixtures for Simulations of Plasma-Assisted Ignition in Turbulent Flows, *Combustion and Flame*, 166, 2016, 133–147.
[46] Starikovskiy, A., Physics and Chemistry of Plasma-Assisted Combustion, *Philosophical Transactions of the Royal Society A Mathematical, Physical and Engineering Sciences*, 373, 2015, 2048.
[47] Bozhenkov, S.A., Starikovskaia, S.M., Starikovskii, A. Yu., Nanosecond Gas Discharge Ignition of H_2– and CH_4– Containing Mixtures, *Combustion and Flame*, 133(1-2), 2003, 133–146.
[48] Stancu, G.D., Kaddouri, F., Lacoste, D.A., Laux, C.O., Atmospheric Pressure Plasma Diagnostics by OES, CRDS and TALIF, *Journal of Physics D: Applied Physics*, 43, 2010, 124002.
[49] Do, H., Plasma-Assisted Combustion in a Supersonic Flow, Ph. D. Thesis, Department of Mechanical Engineering, Stanford University, Stanford, CA, 2009.
[50] Guerra García, C., High Voltage Repetitive Pulsed Nanosecond Discharges as a Selective Source of Reactive Species, MSc Thesis, Department of Aeronautics and Astronautics, Massachusetts Institute of Technology, Cambridge, MA, 2011.

[51] Do, H., Im, S., Cappelli, M.A., Mungal, M.G., Plasma Assisted Flame Ignition of Supersonic Flows Over a Flat Wall, *Combustion and Flame*, 157(12), 2010, 2298–2305.
[52] Burrows, M.C., Kurkov, A.P., An Analytical and Experimental Study of Supersonic Combustion of Hydrogen in Vitiated Air Stream, *AIAA Journal*, 11(9), 1973, 1217–1218.
[53] Pancheshnyi, S., Eismann, B., Hagelaar, G., Pitchford, L., ZDPlasKin: A New Tool for Plasmachemical Simulations, *Bulletin of the American Physical Society*, 53, 2008.
[54] Hagelaar, G.J.M., Pitchford, L.C., Solving The Boltzmann Equation to Obtain Electron Transport Coefficients and Rate Coefficients for Fluid Models, *Plasma Sources Science and Technology*, 14(4), 2005, 722–733.
[55] Orszag, S. A., Yakhot, V., Flannery, W. S., Boysan, F., Renormalization Group Modeling and Turbulence Simulations, *International Conference on Near-Wall Turbulent Flows*, Arizona, Tempe, 1993.
[56] Menter, F.R., Two-Equation Eddy-Viscosity Turbulence Models for Engineering Applications, *AIAA Journal*, 32(8), 1994, 1598–1605.
[57] Eklund, D.R., Drummond, J. P., Hassan, H. A., Calculation of Supersonic Turbulent Reacting Coaxial Jets, *AIAA Journal*, 28(9), 1990, 1633–1641.
[58] Peters, N., Rogg, B., *Reduced Kinetic Mechanisms for Applications in Combustion Systems*, Springer-Verlag, Berlin Heidelberg, 1993.
[59] ANSYS FLUENT 12.0, *Theory Guide*, ANSYS Inc., 2009.
[60] Yin, Z., Montello, A., Carter, C., Lempert, W., Adamovich, I., Measurements of Temperature and Hydroxyl Radical Generation/Decay in Lean Fuel–Air Mixtures Excited by a Repetitively Pulsed Nanosecond Discharge, *Combustion and Flame*, 160(9), 2013, 1594-1608.
[61] Montello, A., Yin, Z., Burnette, D., Adamovich, I., Lempert, W., Picosecond CARS Measurements of Nitrogen Vibrational Loading and Rotational/Translational Temperature in Nonequilibrium Discharges, *Journal of Physics D: Applied Physics*, 46, 2013, 464002.
[62] Starikovskaia, S.M., Kukaev, E.N., Kuksin, A. Yu., Nudnova, M.M., Starikovskii, A.Yu., Analysis of the spatial uniformity of the combustion of a gaseous mixture initiated by a nanosecond discharge, *Combustion and Flame*, 139(3), 2004, 177–187.
[63] Kosarev, I.N., Aleksandrov, N.L., Kindysheva, S.V., Starikovskaia, S.M., Starikovskii, A. Yu., Kinetics of Ignition of Saturated Hydrocarbons by Nonequilibrium Plasma: CH4-Containing Mixtures, *Combustion and Flame*, 154(3), 2008, 569–586.
[64] Brown, P.N., Hindmarsh, A.C., Reduced Storage Matrix Methods in Stiff ODE Systems, *Applied Mathematics and Computation*, 31, 1989, 40–91.
[65] Jachimowski, C.J., An Analytical Study of the Hydrogen-Air Reaction Mechanism with Application to Scramjet Combustion, NASA Langley Research Center Hampton, VA, United States, 1988.
[66] Alves, L.L., Coche, P., Ridenti, M.A., Guerra, V., Electron Scattering Cross Sections for The Modelling of Oxygen-Containing Plasmas, *The European Physical Journal D,* 70, 124, 2016.
[67] Yoon, J.-S., Song, M.-Y., Han, J.-M., Hwang, S.H., Chang, W.-S., Lee, B., Itikawa, Y., Cross Sections for Electron Collisions with Hydrogen Molecules, *Journal of Physical and Chemical Reference Data*, 37, 2008, 913–931.
[68] Capitelli, M., Ferreira, C.M., Gordiets, B.F., Osipov, A.I., *Plasma Kinetics in Atmospheric Gases*, Springer-Verlag, Berlin Heidelberg, 2000.
[69] Burrows and Kurkov, Supersonic Combustion: Study #2, NASA, 2021. https://www.grc.nasa.gov/WWW/wind/valid/bk/study02/bk2.html (accessed October 22, 2021).
[70] Mattick, S., Frankel, S., Numerical Modeling of Supersonic Combustion: Validation and Vitiation Studies Using FLUENT, American Institute of Aeronautics and Astronautics, *41st AIAA/ASME/SAE/ASEE Joint Propulsion Conference & Exhibit*, Tucson, Arizona, 2005.
[71] Evans, J., Schexnayder, JR. C., Critical Influence of Finite Rate Chemistry and Unmixedness on Ignition and Combustion of Supersonic H2-Air Streams, American Institute of Aeronautics and Astronautics, *17th Aerospace Sciences Meeting*, New Orleans, LA, U.S.A, 1979.

ORCID iD

Luis F. Alvarez https://orcid.org/0000-0001-5518-5055
Albio D. Gutierrez https://orcid.org/0000-0002-0005-3714

How to cite this article: Alvarez L.F., Gutierrez A.D. A Reduced-Order Simulation Methodology for Nanosecond-Pulsed Plasmas in a Backward-Facing Step Supersonic Combustor Configuration, *J. Appl. Comput. Mech.*, 9(1), 2023, 181–194. https://doi.org/10.22055/jacm.2022.40704.3644